Surfaces and Interfaces 27 (2021) 101462

Contents lists available at ScienceDirect

Surfaces and Interfaces

journal homepage: www.sciencedirect.com/journal/surfaces-and-interfaces

Flue gas separation at organic-inorganic interface under geological conditions

Lin Tao [a,*], Junchen Huang [a], Davoud Dastan [b], Jing Li [a], Xitao Yin [c,*], Qi Wang [a,*]

[a] School of Chemical Engineering and School of Materials and Metallurgy, University of Science and Technology Liaoning, Anshan 114051, Liaoning, China
[b] School of Materials Science and Engineering, Georgia Institute of Technology, Atlanta, GA 30332, United States
[c] School of Physics and Optoelectronic Engineering, Ludong University, Yantai 264000, Shandong, China

ARTICLE INFO

Keywords:
Flue gas
Separation
Calcite
Graphite
Interface

ABSTRACT

Injecting flue gas into geological reservoirs is a promising way to weaken greenhouse effects and achieve some additional benefits. However, for the effect of heterogeneous (organic-inorganic) interfaces on flue gas separation, it seems to be a lack of detailed theoretical and quantitative understanding, especially when metal ions are doped into organic matter. In this study, graphite-calcite (GC) interface was constructed to explore the adsorption behavior of flue gas by multiscale simulations. The adsorption structure, preferential orientation, relative concentration and diffusion coefficient of flue gas were calculated and compared at GC interface with and without calcium impurity. The results show that CO_2 is preferentially adsorbed on heterogeneous surfaces, while N_2 is squeezed into the central region of the interface. We highlight the importance of the number of Ca ions for flue gas separation. When Ca ion exists on graphite surface, CO_2 adsorption capacity is remarkably enhanced. In practical applications, the selectivity parameter of GC interface containing calcium impurity has reached 21, so it has absolute advantages for flue gas separation. Our work affords new insights into flue gas adsorption in more realistic shale reservoirs.

1. Introduction

Problems of global warming caused by a large amount of flue gas emitted by high energy consumption industries are becoming more and more serious. Flue gas, consists of CO_2 and N_2, is an important part of greenhouse gas [1]. To prevent the greenhouse effect, CO_2 capture and separation techniques have been regard as promising methods [2]. Among which, an innovative approach to inject CO_2 into shale reservoirs was proposed and researched [3–5]. On the one hand, this technique can remove CO_2 from flue gas using the depleted gas reservoirs. On the other hand, CO_2 can replace methane in shale slits and generate some accessional benefits (shale gas). Therefore, it is meaningful to explore the adsorption behavior of flue gas in shale reservoirs.

Shale reservoirs are the complicated sedimentary rocks composed of organic and inorganic substances, which has a lot of nanoporous channels [6,7]. Due to the confused reservoir conditions, it is difficult to study the adsorption behaviors by experimental methods [8]. Molecular simulation can reveal the microscopic mechanism of gas-solid interface interaction [9]. Currently, most researchers focus on the adsorption behavior of gas molecules on the single type of slit-pore of shale matrix (organic or inorganic).

For organic reservoirs, two disconnected and independent graphite slabs are typically regarded as slit pores to represent the complicated nanopore [3,7,10–12]. Liu et al. [3] simulated the adsorption selectivity of CO_2 from CO_2/N_2 mixture in a perfect graphite basal nanopore at 298 K. The results indicated that the interaction energy between CO_2 and the graphite surface is bigger than that between N_2 and the graphite surface. Besides, Wu et al. [11] reported the mechanism about displacement of methane in carbon nano-channel by molecular dynamics (MD) simulation. Their findings demonstrated that the adsorption ability of CO_2 is powerful than that of methane, and CO_2 can displace the adsorbed methane. Furthermore, Yuan et al. [7] revealed the evolution processes for enhanced recovery of methane with CO_2 via MD simulation. The results proved that desorption of methane by CO_2 injection depends on the displacement angle.

For inorganic reservoirs, quartz, clay and calcite are the general constituent substances [6]. Sun et al. [13] described the adsorption property of methane and CO_2 in quartz nanopore by MD simulation. They found the apparent competitive adsorption behavior of CO_2 over methane on nanopore surface in the temperature range of 313-353 K,

* Corresponding authors.
E-mail addresses: taolin_phd@163.com (L. Tao), yxtaj@163.com (X. Yin), wangqi8822@sina.com (Q. Wang).

https://doi.org/10.1016/j.surfin.2021.101462
Received 22 November 2020; Received in revised form 4 September 2021; Accepted 7 September 2021
Available online 15 September 2021

because of interactions between CO_2 and quartz surface. In addition, Zhou et al. [14] investigated the mechanism of adsorption of CO_2 and methane in kaolinite clay via Monte Carlo simulation. They observed two adsorption layers on kaolinite surface, and the selectivity parameter over 7 has been found due to the bigger adsorption ability of CO_2 than methane. Furthermore, Franco [15] and Santos [16] used MD simulation to predict the adsorption behaviors of CO_2 and methane as well as their diffusion behaviors on calcite surface. On this basis, Tao et al. [17] described the kinetic information of CO_2 adsorption on calcite surface by an experiment-simulation collaborative method [18,19].

However, the above mentioned studies have not actually represented geological conditions due to a single type of shale matrix. To further understand shale reservoirs, organic-inorganic models should be considered, this is because many organic and inorganic matters coexist in actual reservoirs [20]. For this reason, Chen et at. [21] constructed the graphite-montmorillonite slit pore to study the adsorption behavior of CH_4 and CO_2 by MD simulation. However, under geological conditions, graphite is idealized as organic reservoirs, which cannot represent the real environment, because the metal ion impurities will be doped into organic matters. To the best of the authors' knowledge, the study of flue gas adsorption behavior on heterogeneous interfaces containing metal ion impurities is blank.

In this study, multiscale simulations were performed to compare the adsorption characteristics of flue gas at organic-inorganic interface with and without metal ion impurity at different temperatures. First of all, the adsorption behaviors of flue gas at heterogeneous interface were shown in detail to intuitively understand the adsorption habits of gas molecules, and the relative concentrations of flue gas at the interface were quantified. Furthermore, the diffusion coefficients were calculated by Einstein diffusion law, which illustrates the effect of heterogeneous nanopore on confined fluids. Next, the electronic properties of gas on organic and inorganic surfaces were calculated by density functional theory (DFT) to acquire the physicochemical heterogeneity (e.g. electron density distribution, adsorption energy and adsorption distance). Finally, in order to quantitatively evaluate the separation performance of flue gas at heterogeneous interface, the selectivity parameter was calculated. This study provides new insights into flue gas adsorption in more realistic shale reservoirs.

2. Methods

2.1. Organic-inorganic interface model

Given that slit-shaped pore of shale reservoir was proved by scanning electron microscopy [22,23], the organic-inorganic nanopore as well as its relevant parameters were defined and two gas molecules were illustrated as shown in Fig. 1. Calcite is one of the primary components in shale reservoirs and the (104) cleave surface for calcite is the most stable crystallographic plane [17,24], so three layers of (104) cleave surface were used to represent inorganic matter. Besides, kerogen is extensive simulated using graphite and practically consistent with experimental results [4,25–27], so graphite is selected as organic matter. Therefore, organic-inorganic interface is represented by graphite-calcite (GC) model.

Graphite consists of 3 parallel independent graphene sheets, in which the interlayer distance is 3.35 Å. Previous studies have testified that 3 layers of graphene sheet are enough due to a weak interaction between the third graphene and gas molecules [3,10,28]. Binary gas (flue gas) of N_2 and CO_2 in the 1:1 ratio was flown into a 20 Å vacuum space at organic-inorganic interface. Significantly, for organic matter containing the metal ion impurities, doped Ca ion was used as the simple model [29]. Fig. 1 shows a inset of the 8.52 Å × 9.84 Å Ca-graphene sheet. In detailed, two adjacent carbon atoms were deleted to form a "5-8-5" type double vacancy, and then the Ca atom was anchored at this vacancy [29]. Hence, GC interface containing Ca ion impurity is represented by Ca-GC interface.

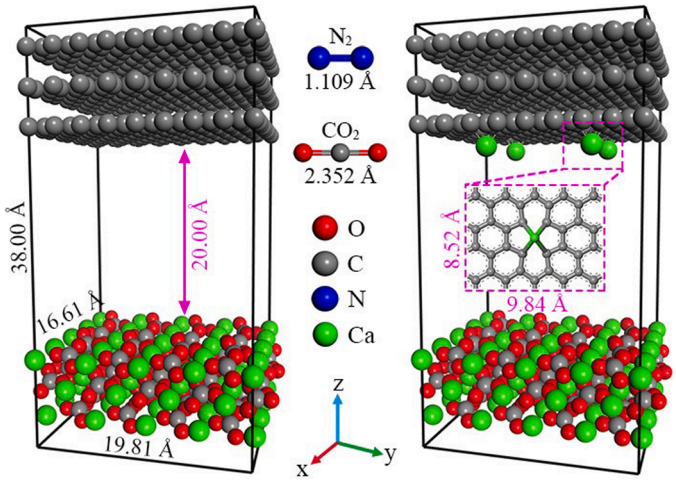

Fig. 1. Models and structure parameters for GC and Ca-GC interfaces. The atomic designations are O (red), C (gray), N (blue), and Ca (green).

To assess the stability of Ca atom on graphite, the binding energy and cohesive energy were calculated. In detailed, if the binding energy between Ca atom and graphite is higher than its cohesive energy of bulk metal, then it is regarded as a stable structure [29]. Based on our calculation, the binding energy between Ca atom and graphite is much lower than its corresponding cohesive energies , denoting that it is prefer to format a stable structure between the Ca atom and graphite, rather than to aggregate on graphite surface.

2.2. Molecular dynamics simulation

The COMPASS force field was used to obtain the adsorption behaviors of flue gas at organic-inorganic interface within Forcite module [30,31]. This force field based on the first *ab-initio* force field can precisely predict thermophysical and structural features for many organic and inorganic materials. The short-range van der Waals was calculated by the Lennard-Jones 9-6 function with the atom-based techniques. The long-range electrostatic interlayer was evaluated by the Columbic interactions with Ewald method. Temperatures of 298, 323, 373, and 423 K were selected to represent the ture reservoirs. The temperature was controlled by Nose thermostat [32]. The constant NVT parameters were used for all MD simulations. The total calculation steps was 5×10^6 in each MD simulation. The time step and the whole simulation time were 1 fs and 5 ns, respectively. The equilibration was achieved in the first 4 ns, and then data analysis was achieved in the last 1 ns. Three independent runs of 1 ns after the equilibration were performed to get the statistical analysis for every single structure.

2.3. First-principle calculation

Based on DFT, electronic properties of flue gas on calcite and graphene surfaces were calculated by $Dmol^3$ module [33,34]. The exchange-correlation interaction was calculated by the generalized gradient approximation (GGA) with the Perdew-Burke-Ernzerhof (PBE) exchange functional [35]. The dispersion-corrected DFT (DFT-D) method with the Grimme vdW correction was adopted to accurately describe weak interactions in this work [36]. The real-space global cut-off radius was 4.9 Å. Based on the Monkhorst-Pack scheme, the Brillouin zone was sampled by 2 × 1 × 1 k-points. The 20 Å vacuum region perpendicular to calcite, graphene, and Ca-graphene surfaces were used to avoid interactions between periodic systems. A two-site model with Lennard-Jones parameters was used to define the neutral N_2 molecule, and a three-site model with three partial charges was evaluated for CO_2 molecule [37].

3. Results and discussion

3.1. Adsorption behavior of flue gas at heterogeneous interfaces

In this section, to explore the differences in the adsorption flue gas at GC and Ca-GC interfaces, snapshots of flue gas adsorbed on heterogeneous surfaces were first shown at different temperatures. Then, the adsorption configurations were described by preferential orientation of CO_2 and N_2. Next, the relative concentrations were calculated to quantitatively characterize the adsorption of two gases at the organic-inorganic interface. Finally, the diffusion coefficients were used to analyze the diffusion behavior of flue gas on heterogeneous surfaces.

3.1.1. Adsorption structure

Fig. 2 shows snapshots of flue gas adsorbed at GC and Ca-GC interfaces under different temperatures. For GC interface under low temperature (Fig. 2**a**), CO_2 molecules are tightly adsorbed on the calcite surface, and regularly adsorbed on the Ca ion sites, which is consistent with previous work [17,38,39]. On graphite surface, CO_2 molecules present the horizontal adsorption configuration. Under the condition that GC surfaces are occupied by CO_2 molecules, N_2 molecules are squeezed into the central region of the pore and present a free gas state. With increasing temperature (Fig. 2**a-d**), some CO_2 molecules adsorbed on the calcite surface are gradually desorbed to become a free phase. Moreover, the desorption of CO_2 on graphite surface is more obvious, which leaves a lot of vacancies, resulting in the diffusion of N_2 to graphite surface.

At Ca-GC interface (Fig. 2**e**), the number of CO_2 molecules adsorbed on calcite surface is almost similar with that at GC interface, but the number of CO_2 on Ca-graphite surface is increased compared with graphite surface. Interestingly, CO_2 molecules are vertically adsorbed at the Ca ion points on graphite surface. N_2 molecules are still mainly confined in the middle region of the interface and distributed randomly. As the temperature increases (Fig. 2**e-h**), CO_2 molecules are desorbed slowly from the Ca-GC surfaces, causing a small amount of N_2 molecules to enter Ca-graphite surface. However, the number of CO_2 molecules adsorbed on Ca-graphite surface is greater than that of CO_2 on graphite surface. Besides, N_2 molecules still can not enter the calcite surface. In brief, the adsorption behaviors of CO_2 are strengthened at the real interface.

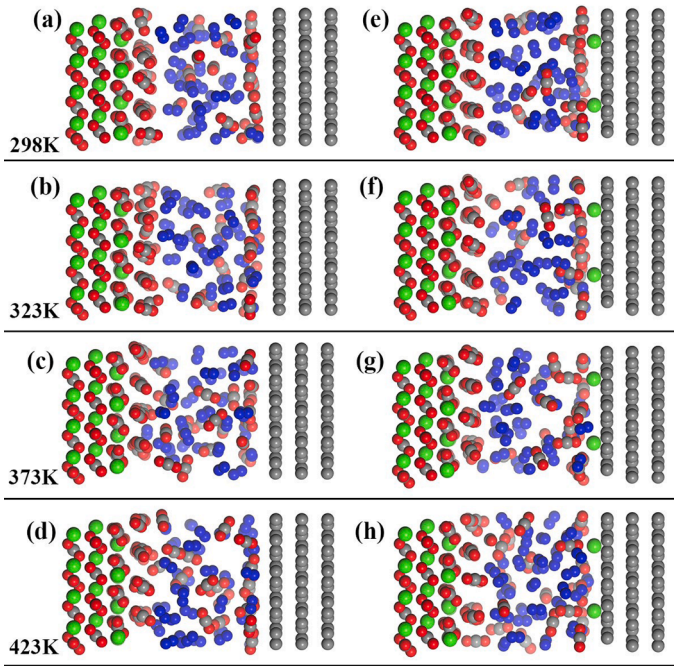

Fig. 2. Snapshots of flue gas adsorbed at GC (a)-(d) and Ca-GC (e)-(h) interfaces under different temperatures.

3.1.2. Preferential orientation

In order to understand the effect of surface heterogeneity on gas adsorption configuration, probability distribution of preferential orientation of CO_2 and N_2 was calculated. First of all, preferential orientation is defined as the angle θ (acute angle) formed between the gas molecular framework and the surface (Fig. 3**a**). When θ is 0°, gas molecule is parallel to the surface; when θ is 90°, gas molecule is perpendicular to the surface. According to the results of Fig. 2, we counted three special preferential orientations of flue gas molecules. Fig. 3**b** shows the ratio for the angle θ of gas molecules at GC and Ca-GC interfaces under the temperature of 298 K.

At GC interface, CO_2 molecules have two special adsorption orientations, to be distributed at the angle θ of ~45° and ~0°. This proves that CO_2 molecules are vertical on calcite surface and lie flat on graphite surface under the strong interaction. Thereinto, the amount of CO_2 distributed on calcite surface is larger than that on graphite surface, which is consistent with the results in Fig. 2**a**. N_2 molecules show a widely distributed free gas state because of the weak interaction. At Ca-GC interface, N_2 molecules still maintain the bulk phase structure. CO_2 molecules appear a new angle of ~90° in addition to ~45° and ~0°. It means that CO_2 molecules emerge a perpendicular adsorption configuration on Ca-graphite surface due to the presence of Ca ions (Fig. 2**e**). Especially, the ratio of the three configurations (~90°, ~45°, and ~0°) at Ca-GC interface is greater than that of two configurations (~45° and ~0°) at GC interface. This means there is an increase in the number of CO_2 molecules under real reservoirs.

3.1.3. Relative concentration

To quantitatively describe the adsorption behavior of flue gas on heterogeneous surfaces, the relative concentrations [10,40] were calculated at GC and Ca-GC interfaces under different temperatures. At GC interface (Fig. 4**a**), CO_2 forms two distinct adsorption layers, and the relative concentration of CO_2 on calcite is larger than that of CO_2 on graphite. N_2 is not adsorbed and becomes a free gas state in the central region of the interface. Due to the low relative concentration of CO_2 on graphite surface, some N_2 molecules drill into the vacancies on graphite surface. As the temperature increases (Fig. 4), the flue gas is gradually desorbed from the GC interface.

At Ca-GC interface (Fig. 4**a**), the relative concentration of CO_2 on calcite surface is almost unaffected. However, on Ca-graphite surface, the relative concentration of CO_2 increases significantly, which results in more N_2 being squeezed in the central region of the interface. Accordingly, the number of nitrogen molecules on graphite surface decreases. It suggests that the presence of impurity Ca ions enhances the adsorption capacity of CO_2. As the temperature rises (Fig. 4), the relative concentration of the flue gas at Ca-GC interface decreases slowly, but the relative concentration of CO_2 on Ca-graphite surface is still higher than that of CO_2 on graphite. Hence, the results confirm that CO_2 has better adsorption ability in real shale reservoirs.

3.1.4. Diffusion behavior

To illustrate the effects of heterogeneous nanopore on confined fluids, the mean square displacement (MSD) method [17] and Einstein diffusion law [41] were used to calculate the the diffusion coefficient, which can describe the diffusion behaviors of flue gas at GC and Ca-GC interfaces. Specific formulas are as follows:

$$MSD(t) = \frac{1}{N}\sum_{i=1}^{N}\left\langle |r_i(t) - r_i(0)|^2 \right\rangle \quad (1)$$

$$D_S = \frac{1}{6}\lim_{t\to\infty}\frac{d}{dt}\sum_{i}^{n}\left\langle |r_i(t) - r_i(0)|^2 \right\rangle \quad (2)$$

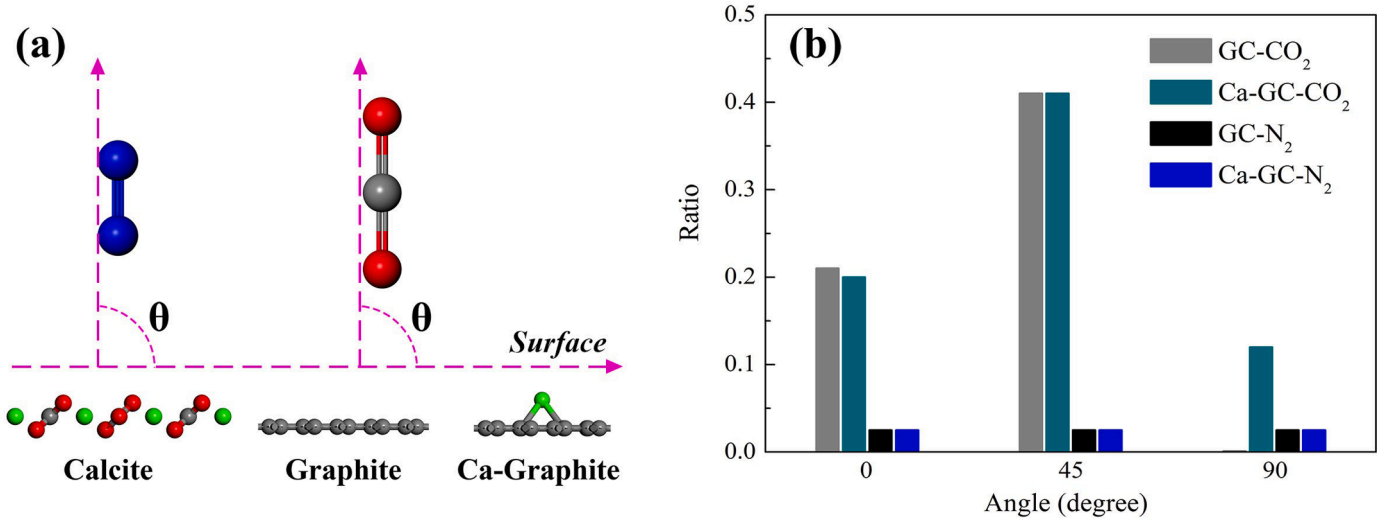

Fig. 3. (a) Illustration for CO_2 and N_2 orientations on different surfaces. (b) Ratio for the angle θ of N_2 and CO_2 molecules on GC and Ca-GC surfaces at 298 K.

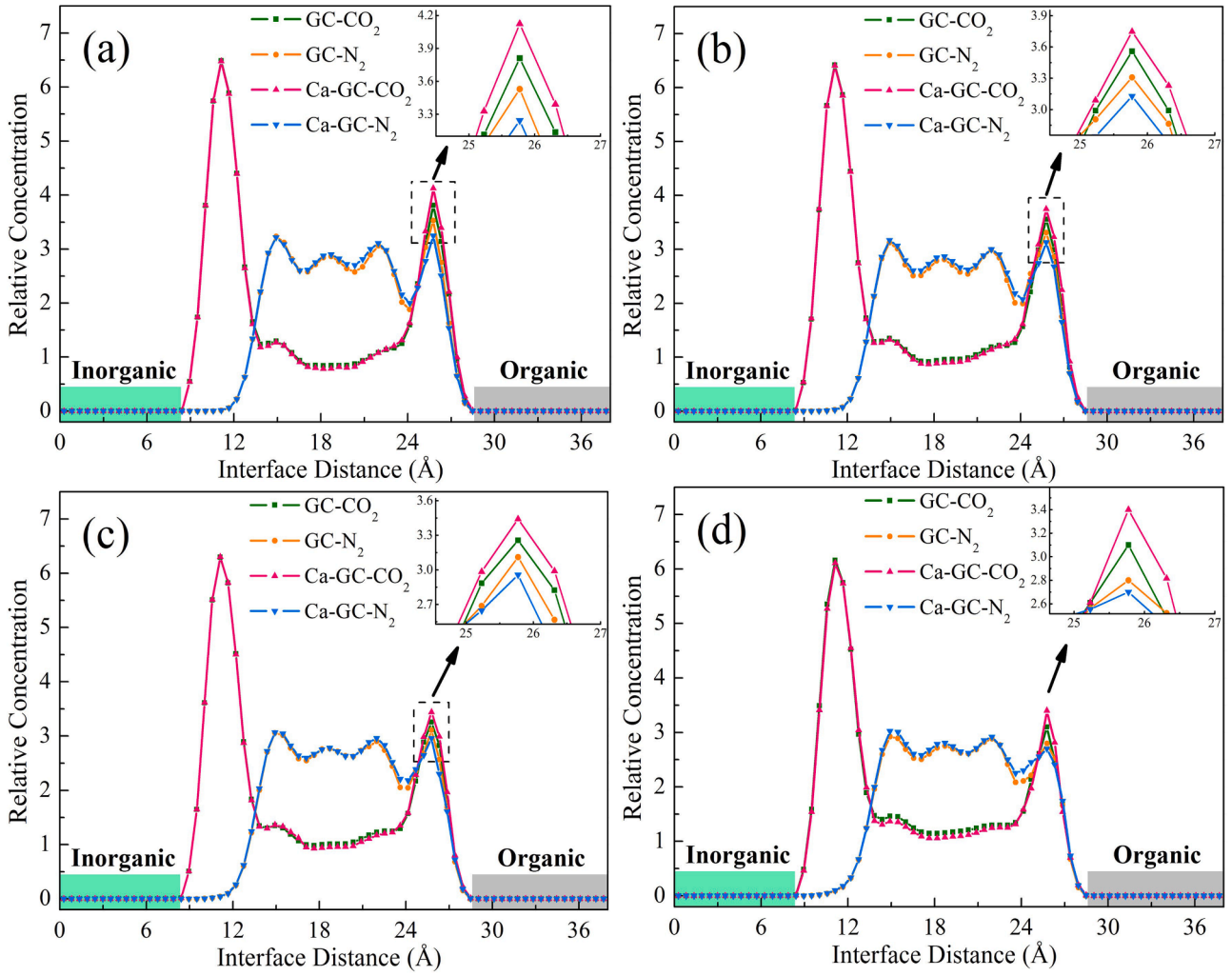

Fig. 4. Relative concentration of flue gas adsorbed at GC and Ca-GC interfaces under different temperatures. (a) 298 K, (b) 323 K, (c) 373 K, and (d) 423 K.

where N is the number of flue gas molecules, $r_i(t)$ is the position of flue gas molecules at the time t, and $r_i(0)$ is the initial position.

The larger diffusion coefficient denotes the higher diffusivity of flue gas molecules. At GC interface (Fig. 5), N_2 has the strongest diffusivity under various temperatures. It denotes that the interaction between the heterogeneous surface and N_2 is very weak, while the interaction with CO_2 is quite strong. As the temperature rises, all the diffusion coefficients become larger, it indicates that temperature promotes the gas

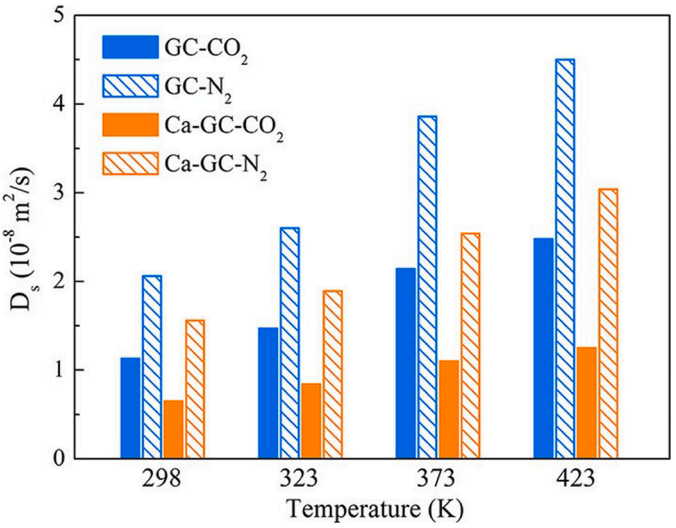

Fig. 5. Diffusion coefficients of CO_2 and N_2 adsorbed at GC and Ca-GC interfaces under different temperatures.

diffusion. At Ca-GC interface (Fig. 5), N_2 also has a powerful diffusivity under different temperatures and it is positively correlated with temperature, but the diffusivity of N_2 at Ca-GC interface is clearly weak than that of N_2 at GC interface. It suggests that the presence of Ca ions apparently enhances the adsorption ability of N_2. By contrast, the diffusivity of CO_2 at the Ca-GC interface is smallest. Therefore, this strongly indicates that the diffusion behavior of CO_2 in real shale reservoirs is weaker than that of N_2.

3.2. Adsorption mechanism of flue gas at heterogeneous interfaces

Section 3.1 shows that the adsorption capacity of CO_2 on calcite surface is larger than that of CO_2 on Ca-graphite surface, while N_2 keeps the free gas state. Moreover, the diffusion coefficient of CO_2 is significantly reduced due to the presence of Ca ion. In order to explain the underlying mechanism, the first principle is used to explore the gas-solid interface. In this section, we comprehensively discussed the adsorption details of flue gas on heterogeneous surfaces through adsorption energy, adsorption distance and electron density distribution.

First of all, according to the previous research [12,29,39,42], the original adsorption configurations of CO_2 and N_2 on heterogeneous surfaces are constructed as shown in Fig. 6. Then, to calculate the adsorption energy, it can be defined as

$$E_{ads} = E_{total} - \left(E_{surface} + E_{gas}\right) \quad (3)$$

where E_{ads} is the adsorption energy of flue gas on heterogeneous surfaces (eV), E_{total} is the single point energy of flue gas on heterogeneous surfaces (eV), $E_{surface}$ is the single point energy of heterogeneous surfaces (eV), and E_{gas} is the single point energy of flue gas (eV). A more negative value indicates a stronger interaction between flue gas and the heterogeneous surfaces. As shown in Fig. 7**a,b**, both CO_2 and N_2 are adsorbed vertically on calcite surface. The adsorption distance of CO_2 on calcite surface is shorter than that of N_2 on calcite surface. It can be attributed to the stronger electrostatic interaction between CO_2 and calcite surface than that between N_2 and calcite surface. Thus, no N_2 molecules can be found on calcite surface in Fig. 4. Besides, no electrons overlap between flue gas and calcite surface is found by electron density distribution map. It confirms that the flue gas shows physisorption on calcite surface.

Fig. 7**c,d** shows that both CO_2 and N_2 lie flat on graphene surface, and have similar adsorption distances. Nevertheless, the adsorption energy of CO_2 on graphene surface is bigger than that of N_2 on graphene surface. Therefore, CO_2 is preferentially adsorbed to graphite surface (Fig. 4). In addition, the flue gas also shows physisorption on graphene surface based on the electron density distribution map.

When Ca ion exists on the graphene surface, the adsorption energy of CO_2 on graphene surface is evidently enhanced and the adsorption distance is clearly shortened (Fig. 7**c,e**). N_2 becomes a perpendicular adsorption configuration and the adsorption energy is relatively stable (Fig. 8**d,f**). Significantly, the adsorption energy of CO_2 on Ca-graphene is stronger than that of CO_2 on calcite surface (Fig. 7**a,e**). Interestingly, the relative concentration of CO_2 on the Ca-graphite is lower than that of CO_2 on calcite surface (Fig. 4). To explain this phenomenon, we calculated the density of Ca ion on calcite and graphite surfaces. This is because CO_2 with Ca ion is one-to-one adsorption according to our previous study [17,38,42]. In detail, the surface density of Ca ions on calcite surface was calculated as follow (Fig. 1): the number of Ca ions on calcite surface (16) divided by the area of calcite surface (16.61 Å × 19.81 Å). Similarly, the surface density of Ca ions on graphite surface was calculated as follow: the number of Ca ions on graphite surface (4) divided by the area of graphite surface (16.61 Å × 19.81 Å).

The results show that the density of Ca ion on calcite surface is 4.863 nm^{-2}, and the density of Ca ion on graphite surface is 1.216 nm^{-2}. This indicates that the number of Ca ions significantly affects CO_2 adsorption capacity. Overall, CO_2 is physically adsorbed at Ca-GC interfaces by the

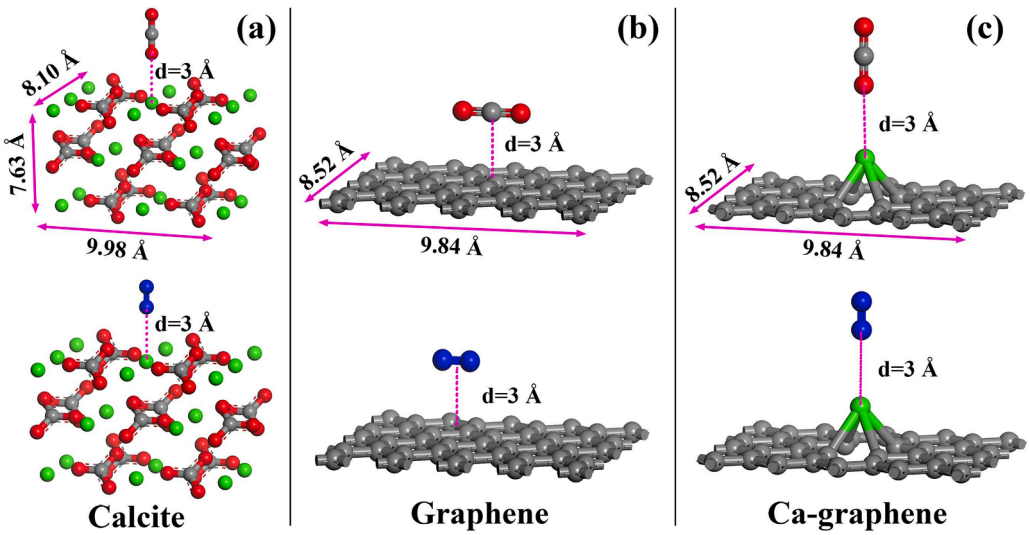

Fig. 6. Original adsorption configuration of flue gas on heterogeneous surfaces. (a) Calcite surface, (b) Graphene surface, and (c) Ca-graphene surface.

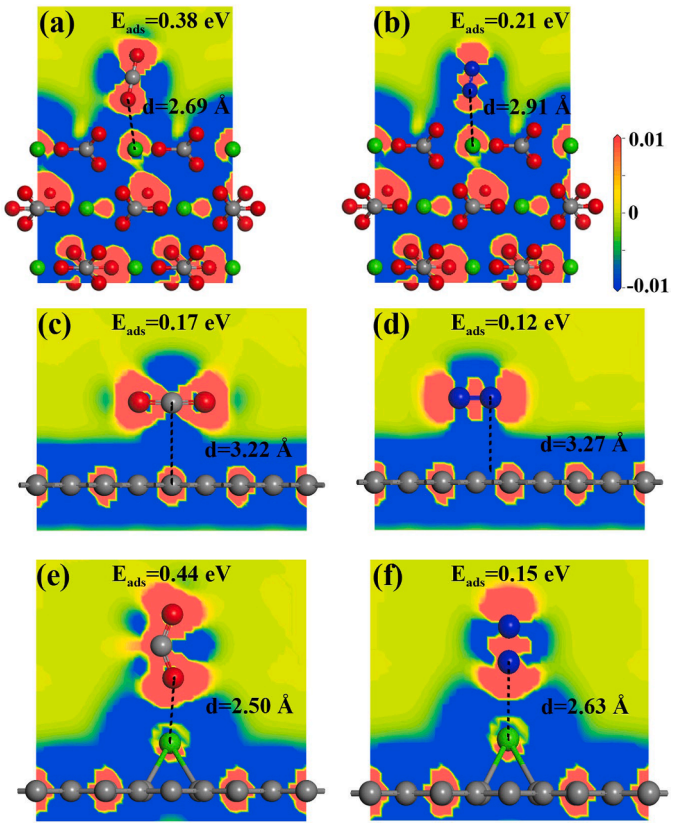

Fig. 7. Electron density distribution, adsorption energy and adsorption distance of flue gas on heterogeneous surfaces. The densities are drawn with an isosurface, and the range of isovalue is set to be -0.01 to 0.01. (a) CO_2 on calcite surface, (b) N_2 on calcite surface, (c) CO_2 on graphene surface, (d) N_2 on graphene surface, (e) CO_2 on Ca-graphene surface, and (f) N_2 on Ca-graphene surface.

strong electrostatic interactions between the O atom in CO_2 and the Ca ion in calcite. Because the adsorption energy of CO_2 on heterogeneous surface is larger than that of N_2, it is preferentially to adsorb CO_2 from flue gas. In addition, the stronger the adsorption energy is, the worse the diffusion ability becomes. The more the number of Ca ions possesses, the bigger the CO_2 adsorption capacity is.

3.3. Application of flue gas separation: selectivity parameter

In practical applications, the selectivity parameter is an important index because it is the most direct parameter to quantify the competitive adsorption performance of mixed gases. The selectivity parameter S of CO_2 over N_2 at GC and Ca-GC interfaces can be defined as follows [1]:

$$S_{CO_2/N_2} = \frac{x_{CO_2}/x_{N_2}}{y_{CO_2}/y_{N_2}} \quad (4)$$

where x is the molar fraction of the gas constituent in the adsorbed phase and y is the molar fraction of the gas constituent in the bulk phase. If the selectivity parameter S is greater than 1, it denotes that CO_2 preferentially adsorbs over N_2 throughout the adsorption process.

Therefore, we intuitively compared the selectivity parameters of some typical adsorbent materials in Fig. 8 [1,3,43–57]. It can be found that a portion of porous materials have good separation performance at room temperature, while the selectivity decreases immediately once the temperature increases. However, the selectivity parameter of GC increases with increasing temperature and can also reach moderate level at room temperature. Specially, the selectivity parameter of Ca-GC is significantly better than that of GC at the whole temperature, in which the selectivity parameter exceeds 20 at 423 K. Therefore, under the high temperature and complex shale reservoirs environment, the separation performance of flue gas at Ca-GC interface is definitely better than that of most adsorbent materials. This proves that the presence of Ca ions contributes to flue gas separation.

4. Conclusion

Multiscale simulations are used to study the difference in the adsorption behavior of flue gas at GC and Ca-GC interfaces. MD simulation results show that CO_2 is preferentially adsorbed on GC surface, while N_2 is squeezed into the central region of the interface. At Ca-GC interface, the adsorption of CO_2 on graphite surface is enhanced due to the presence of Ca ion. Further, according to the adsorption orientation of gas molecules, CO_2 molecules present the angle of 45° erect adsorption configuration on calcite surface, the state of lying flat on graphite surface, and a 90° vertical adsorption structure on Ca-graphite surface. Besides, the results of relative concentration confirm the positive effect of Ca ion on CO_2 adsorption capacity, in which the concentration of CO_2 on Ca-graphite surface is higher than that of graphite. Meanwhile, the adsorption capacities of flue gas at GC and Ca-GC interfaces are negatively correlated with temperature. Nevertheless, the diffusions of flue gas at GC and Ca-GC interfaces are positively

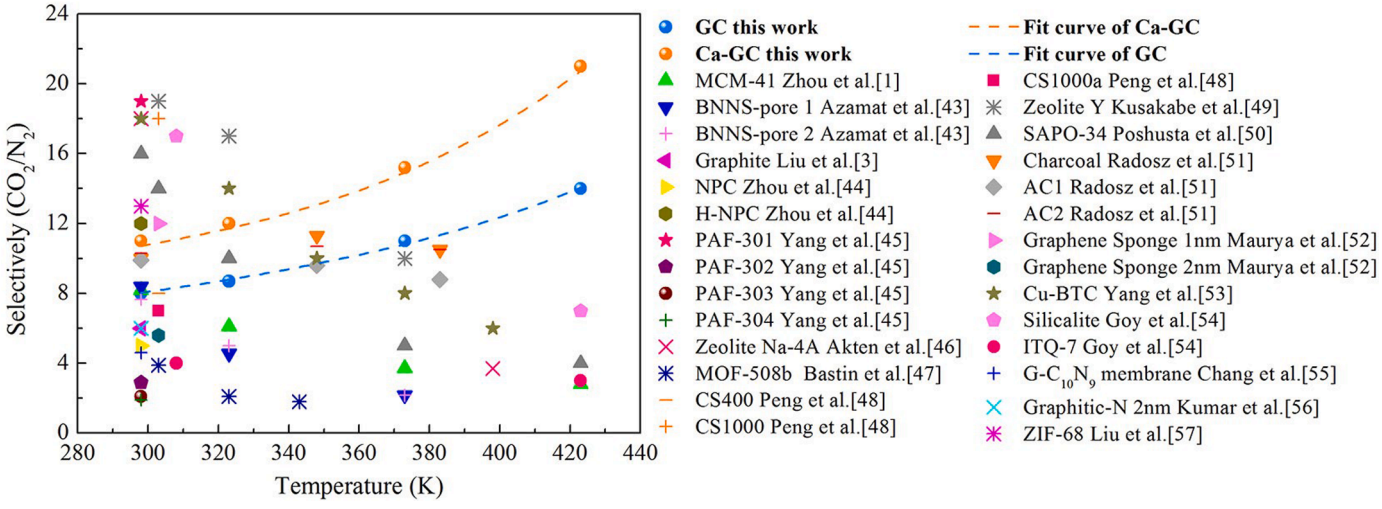

Fig. 8. Selectivity parameters of flue gas on various materials at different temperatures.

correlated with temperature. To clarify the separation mechanism of flue gas at GC and Ca-GC interfaces, DFT calculation results show that the adsorption energy of CO_2 on calcite surface is obviously larger than that of N_2, so the flue gas can be separated effectively. When the flue gas is adsorbed on graphite surface, the adsorption energy of CO_2 is similar with that of N_2, so the separation performance is relatively poor. For the first time, we highlight the importance of the number of Ca ions for flue gas separation. When Ca ion exists on graphite surface, the adsorption energy of CO_2 is significantly increased (beyond the interaction between CO_2 and calcite), but the adsorption capacity is lower than that of calcite. This is because the density of Ca ions on graphite is lower than that on calcite. For practical applications, the selectivity parameter of Ca-GC interface has reached 21, so it has absolute advantages for flue gas separation.

Author statement

Lin Tao: Conceptualization, Methodology, Formal analysis, Writing - original draft. **Junchen Huang**: Formal analysis, Writing - review & editing. **Davoud Dastan**: Formal analysis, Writing - review & editing. **Jing Li**: Resources, Visualization. **Xitao Yin**: Conceptualization, Supervision, Resources. **Qi Wang**: Methodology, Writing - review & editing, Software, Resources.

Declaration of Competing Interest

The authors declare that they have no known competing financial interests or personal relationships that could have appeared to influence the work reported in this paper.

Acknowledgements

We are very grateful for the support of the National Natural Science Foundation of China (Fund number: 51874169, 51634004, and 51974157).

References

[1] S. Zhuo, Y. Huang, J. Hu, H. Liu, Y. Hu, J. Jiang, Computer Simulation for Adsorption of CO2, N2and Flue Gas in a Mimetic MCM-41, J. Phys. Chem. C 112 (2008) 11295–11300.
[2] D.W. Keith, Why Capture CO2 from the Atmosphere? Science 325 (2009) 1654–1655.
[3] Y. Liu, J. Wilcox, Molecular simulation studies of CO2 adsorption by carbon model compounds for carbon capture and sequestration applications, Environ. Sci. Technol. 47 (2013) 95–101.
[4] M. Zhang, S. Zhan, Z. Jin, Recovery mechanisms of hydrocarbon mixtures in organic and inorganic nanopores during pressure drawdown and CO2 injection from molecular perspectives, Chem. Eng. J. 382 (2020), 122808.
[5] A. Hamza, I.A. Hussein, M.J. Al-Marri, M. Mahmoud, R. Shawabkeh, S. Aparicio, CO2 enhanced gas recovery and sequestration in depleted gas reservoirs: A review, J. Petrol. Sci. Eng. 196 (2021), 107685.
[6] Z. Ma, P.G. Ranjith, Review of application of molecular dynamics simulations in geological sequestration of carbon dioxide, Fuel 255 (2019), 115644.
[7] Q. Yuan, X. Zhu, K. Lin, Y.P. Zhao, Molecular dynamics simulations of the enhanced recovery of confined methane with carbon dioxide, Phys. Chem. Chem. Phys. PCCP 17 (2015) 31887–31893.
[8] Y. Ma, G. Lu, C. Shao, X. Li, Molecular dynamics simulation of hydrocarbon molecule adsorption on kaolinite (0 0 1) surface, Fuel 237 (2019) 989–1002.
[9] Z. Tian, S. Dai, D.-e. Jiang, What can molecular simulation do for global warming? Wiley Interdisciplin. Rev. Comput. Mol. Sci. 6 (2016) 173–197.
[10] X. Yang, W. Zhou, X. Liu, Y. Yan, A multiscale approach for simulation of shale gas transport in organic nanopores, Energy 210 (2020), 118547.
[11] H. Wu, J. Chen, H. Liu, Molecular Dynamics Simulations about Adsorption and Displacement of Methane in Carbon Nanochannels, J. Phys. Chem. C 119 (2015) 13652–13657.
[12] K. Kwac, J.H. Lee, J.W. Choi, Y. Jung, Computational Analysis of Pressure-Dependent Optimal Pore Size for CO2 Capture with Graphitic Surfaces, J. Phys. Chem. C 120 (2016) 3978–3985.
[13] H. Sun, W. Sun, H. Zhao, Y. Sun, D. Zhang, X. Qi, Y. Li, Adsorption properties of CH4 and CO2 in quartz nanopores studied by molecular simulation, RSC Adv. 6 (2016) 32770–32778.
[14] W. Zhou, H. Wang, Y. Yan, X. Liu, Adsorption Mechanism of CO2/CH4 in Kaolinite Clay: Insight from Molecular Simulation, Energy Fuels 33 (2019) 6542–6551.
[15] L.F. Franco, M. Castier, I.G. Economou, Anisotropic parallel self-diffusion coefficients near the calcite surface: A molecular dynamics study, J. Chem. Phys. 145 (2016), 084702.
[16] M.S. Santos, L.F.M. Franco, M. Castier, I.G. Economou, Molecular Dynamics Simulation of n-Alkanes and CO2 Confined by Calcite Nanopores, Energy Fuels 32 (2018) 1934–1941.
[17] L. Tao, J. Huang, X. Yin, Q. Wang, Z. Li, G. Wang, B. Cui, Adsorption Kinetics of CO2 on a Reconstructed Calcite Surface: An Experiment-Simulation Collaborative Method, Energy Fuels 33 (2019) 8946–8953.
[18] X.-T. Yin, L. Tao, Fabrication and gas sensing properties of Au-loaded SnO2 composite nanoparticles for low concentration hydrogen, J. Alloys Compd. 727 (2017) 254–259.
[19] X.-T. Yin, J. Li, D. Dastan, W.-D. Zhou, H. Garmestani, F.M. Alamgir, Ultra-high selectivity of H2 over CO with a p-n nanojunction based gas sensors and its mechanism, Sens. Actuators B 319 (2020), 128330.
[20] S. Wang, Q. Feng, M. Zha, F. Javadpour, Q. Hu, Supercritical methane diffusion in shale nanopores: effects of pressure, mineral types, and moisture content, Energy Fuels 32 (2017) 169–180.
[21] C. Chen, J. Sun, Y. Zhang, J. Mu, W. Li, Y. Song, Adsorption characteristics of CH4 and CO2 in organic-inorganic slit pores, Fuel 265 (2020), 116969.
[22] K. Wu, Z. Chen, X. Li, Real gas transport through nanopores of varying cross-section type and shape in shale gas reservoirs, Chem. Eng. J. 281 (2015) 813–825.
[23] A. Afsharpoor, F. Javadpour, Liquid slip flow in a network of shale noncircular nanopores, Fuel 180 (2016) 580–590.
[24] W. Zhang, Q. Feng, S. Wang, X. Xing, Z. Jin, CO2-regulated octane flow in calcite nanopores from molecular perspectives, Fuel 286 (2021), 119299.
[25] Z. Jin, A. Firoozabadi, Thermodynamic Modeling of Phase Behavior in Shale Media, SPE J. 21 (2016) 190–207.
[26] Y. Liu, J. Wilcox, Molecular simulation of CO2 adsorption in micro- and mesoporous carbons with surface heterogeneity, Int. J. Coal Geol. 104 (2012) 83–95.
[27] K. Mosher, J. He, Y. Liu, E. Rupp, J. Wilcox, Molecular simulation of methane adsorption in micro- and mesoporous carbons with applications to coal and gas shale systems, Int. J. Coal Geol. 109-110 (2013) 36–44.
[28] P. Billemont, B. Coasne, G. De Weireld, An experimental and molecular simulation study of the adsorption of carbon dioxide and methane in nanoporous carbons in the presence of water, Langmuir 27 (2011) 1015–1024.
[29] A. Liu, J. Long, S. Yuan, W. Cen, J. Li, Synergetic promotion by oxygen doping and Ca decoration on graphene for CO2 selective adsorption, Phys. Chem. Chem. Phys. PCCP 21 (2019) 5133–5141.
[30] H. Sun, P. Ren, J. Fried, The COMPASS force field: parameterization and validation for phosphazenes, Comput. Theor. Polym. Sci. 8 (1998) 229–246.
[31] H. Sun, COMPASS: an ab initio force-field optimized for condensed-phase applications overview with details on alkane and benzene compounds, J. Phys. Chem. B 102 (1998) 7338–7364.
[32] S. Nosé, A molecular dynamics method for simulations in the canonical ensemble, Mol. Phys. 52 (1984) 255–268.
[33] B. Delley, An all-electron numerical method for solving the local density functional for polyatomic molecules, J. Chem. Phys. 92 (1990) 508–517.
[34] B. Delley, From molecules to solids with the DMol 3 approach, J. Chem. Phys. 113 (2000) 7756–7764.
[35] J.P. Perdew, K. Burke, M. Ernzerhof, Generalized Gradient Approximation Made Simple, Phys. Rev. Lett. 77 (1996) 3865–3868.
[36] S. Grimme, Semiempirical GGA-type density functional constructed with a long-range dispersion correction, J. Comput. Chem. 27 (2006) 1787–1799.
[37] J.J. Potoff, J.I. Siepmann, Vapor–liquid equilibria of mixtures containing alkanes, carbon dioxide, and nitrogen, AIChE J. 47 (2001) 1676–1682.
[38] L. Tao, Z. Li, G.-C. Wang, B.-Y. Cui, X.-T. Yin, Q. Wang, Evolution of calcite surface reconstruction and interface adsorption of calcite-CO2 with temperature, Mater. Res. Express 6 (2018), 025035.
[39] L. Tao, J. Huang, D. Dastan, T. Wang, J. Li, X. Yin, Q. Wang, New insight into absorption characteristics of CO2 on the surface of calcite, dolomite, and magnesite, Appl. Surf. Sci. 540 (2021), 148320.
[40] G. Wu, L. He, D. Chen, Sorption and distribution of asphaltene, resin, aromatic and saturate fractions of heavy crude oil on quartz surface: molecular dynamic simulation, Chemosphere 92 (2013) 1465–1471.
[41] A. Einstein, On the movement of small particles suspended in stationary liquids required by the molecularkinetic theory of heat, Ann. D. Phys. 17 (1905) 1.
[42] L. Tao, J. Huang, D. Dastan, T. Wang, J. Li, X. Yin, Q. Wang, CO2 capture and separation on charge-modulated calcite, Appl. Surf. Sci. 530 (2020), 147265.
[43] J. Azamat, A. Khataee, F. Sadikoglu, Separation of carbon dioxide and nitrogen gases through modified boron nitride nanosheets as a membrane: insights from molecular dynamics simulations, RSC Adv. 6 (2016) 94911–94920.
[44] S. Zhou, C. Guo, Z. Wu, M. Wang, Z. Wang, S. Wei, S. Li, X. Lu, Edge-functionalized nanoporous carbons for high adsorption capacity and selectivity of CO2 over N2, Appl. Surf. Sci. 410 (2017) 259–266.
[45] Z. Yang, X. Peng, D. Cao, Carbon dioxide capture by PAFs and an efficient strategy to fast screen porous materials for gas separation, J. Phys. Chem. C 117 (2013) 8353–8364.
[46] E.D. Akten, R. Siriwardane, D.S. Sholl, Monte Carlo Simulation of Single- and Binary-Component Adsorption of CO2, N2, and H2in Zeolite Na-4A, Energy Fuels 17 (2003) 977–983.
[47] L. Bastin, P.S. Bárcia, E.J. Hurtado, J.A.C. Silva, A.E. Rodrigues, B. Chen, A Microporous Metal−Organic Framework for Separation of CO2/N2and CO2/CH4by Fixed-Bed Adsorption, J. Phys. Chem. C 112 (2008) 1575–1581.

[48] X. Peng, S.K. Jain, J.K. Singh, Adsorption and Separation of N2/CH4/CO2/SO2 Gases in Disordered Carbons Obtained Using Hybrid Reverse Monte Carlo Simulations, J. Phys. Chem. C 121 (2017) 13457–13473.
[49] K. Kusakabe, T. Kuroda, A. Murata, S. Morooka, Formation of a Y-Type Zeolite Membrane on a Porous α-Alumina Tube for Gas Separation, Ind. Eng. Chem. Res. 36 (1997) 649–655.
[50] J.C. Poshusta, V.A. Tuan, E.A. Pape, R.D. Noble, J.L. Falconer, Separation of light gas mixtures using SAPO-34 membranes, AIChE J. 46 (2000) 779–789.
[51] M. Radosz, X. Hu, K. Krutkramelis, Y. Shen, Flue-Gas Carbon Capture on Carbonaceous Sorbents: Toward a Low-Cost Multifunctional Carbon Filter for "Green" Energy Producers†, Ind. Eng. Chem. Res. 47 (2008) 3783–3794.
[52] M. Maurya, J.K. Singh, Treatment of Flue Gas using Graphene Sponge: A Simulation Study, J. Phys. Chem. C 122 (2018) 14654–14664.
[53] Q. Yang, C. Xue, C. Zhong, J.-F. Chen, Molecular simulation of separation of CO2 from flue gases in CU-BTC metal-organic framework, AIChE J. 53 (2007) 2832–2840.
[54] A. Goj, D.S. Sholl, E.D. Akten, D. Kohen, Atomistic Simulations of CO2 and N2 Adsorption in Silica Zeolites: The Impact of Pore Size and Shape, J. Phys. Chem. B 106 (2002) 8367–8375.
[55] X. Chang, L. Zhu, Q. Xue, X. Li, T. Guo, X. Li, M. Ma, Charge controlled switchable CO2/N2 separation for g-C10N9 membrane: Insights from molecular dynamics simulations, J. CO2 Utiliz. 26 (2018) 294–301.
[56] K.V. Kumar, K. Preuss, L. Lu, Z.X. Guo, M.M. Titirici, Effect of Nitrogen Doping on the CO2Adsorption Behavior in Nanoporous Carbon Structures: A Molecular Simulation Study, J. Phys. Chem. C 119 (2015) 22310–22321.
[57] B. Liu, B. Smit, Molecular Simulation Studies of Separation of CO2/N2, CO2/CH4, and CH4/N2 by ZIFs, J. Phys. Chem. C 114 (2010) 8515–8522.